Different Ground Spin States in Iron(III) Complexes with Quadridentate Schiff Bases: Synthesis, Crystal Structures, and Magnetic Properties

Rita Hernández-Molina,[1a] Alfredo Mederos,*,[1a] Sixto Dominguez,[1a] Pedro Gili,[1a] Catalina Ruiz-Pérez,[1b] Alfonso Castiñeiras,[1c] Xavier Solans,[1d] Francesc Lloret,[1e] and José Antonio Real*,[1e]

Departamento de Química Inorgánica, Universidad de La Laguna, 38200 La Laguna, Tenerife, Canary Islands, Spain, Departamento de Física Fundamental y Experimental, Universidad de La Laguna, Avenida Astrofísico Francisco Sánchez 34200 La Laguna, Tenerife, Canary Islands, Spain, Departamento de Química Inorgánica, Universidad de Santiago, 15076 Santiago de Compostela, Spain, Departament de Cristal.lografia, Mineralogia i Dipòsits Minerals, Facultat de Geologia, Universitat de Barcelona, 08028 Barcelona, Spain, and Departament de Química Inorgànica, Universitat de València, Dr. Moliner 50, 46100 Burjassot (València), Spain

The synthesis, structure, and magnetic characterization of $[Fe(L^1)(HIm)_2]$ Y (Y = ClO_4^- (**1a**), PF_6^- (**1b**), and BPh_4^- (**1c**)), $[Fe(L^2)(HIm)_2]ClO_4$ (**2a**), $[Fe(L^2)(HIm)_2]ClO_4 \cdot H_2O$ (**2b**), $[NaFe(L^2)(HIm)_2(ClO_4)_2]$ (**2c**), $[Fe(L^3)-(HIm)_2]ClO_4$ (**3**), $[Fe(L^4)(HIm)_2]ClO_4$ (**4a**), and $[Fe(L^4)(HIm)_2]$ $BPh_4 \cdot H_2O$ (**4b**) are reported (L^1 = *N,N′*-3,4-toluenebis(3-ethoxysalicylideneimine), L^2 = *N,N′*-4-chloro-*o*-phenylenebis(3-methoxysalicylideneimine), L^3 = *N,N′*-4-chloro-*o*-phenylenebis(3-ethoxysalicylideneimine), L^4 = *N,N′*-1,2-propylenebis(3-methoxysalicylideneimine), and HIm = imidazole). Compound **1a** crystallizes in the triclinic system, space group $P\bar{1}$, Z = 2, with a = 10.609(3) Å, b = 10.762(3) Å, c = 15.043(3) Å, α = 105.13(2)°, β = 90.67(2)°, and γ = 102.09(2)°. Compound **2c** crystallizes in the monoclinic system, space group $C2/c$, Z = 4, with a = 14.969(6) Å, b = 17.324(6) Å, c = 13.050(10) Å, and β = 100.85(6)°. Compound **4a** crystallizes in the orthorhombic system, space group $P2_12_12_1$, Z = 4, with a = 12.402(2) Å, b = 14.354(2) Å, c = 15.773(2) Å. The structures of **1a** and **4a** are made up of discrete $[Fe(L^1)(HIm)_2]^+$ and $[Fe(L^4)(HIm)_2]^+$ cationic units, while **2c** consists of dinuclear neutral entities $[NaFe-(L^2)(HIm)_2(ClO_4)_2]$. The iron(III) ion is six-coordinated, the equatorial plane being occupied by the cis tetradentate Schiff base and the axial positions by the imidazole ligands. The metal−ligand bond distances as well as the relative orientation of the imidazole ligands are discussed in relation with the spin state of the title compounds. The magnetic properties reveal that **1a−c**, **2a**, **3**, and **4b** are high-spin species while **2c** is a low-spin complex, and **2b** and **4a** display spin-crossover behavior. The thermodynamic model of Slichter and Drickamer was applied to account for the temperature variable high-spin molar fraction deduced from the magnetic behavior. The intermolecular interaction parameter, Γ, the enthalpy, ΔH, and the entropy, ΔS, changes associated with the spin transition of **2b** were estimated as Γ = 1.6 kJ mol^{-1}, ΔH = 12 kJ mol^{-1}, and ΔS = 60 J mol^{-1} K^{-1}.

Introduction

The magnetic properties of mononuclear iron(III) complexes are generally well understood. Iron(III) has the $3d^5$ outer electronic configuration and hence its complexes may be either high-spin ($S = \frac{5}{2}$, HS), intermediate-spin ($S = \frac{3}{2}$, IS), or low-spin ($S = \frac{1}{2}$, LS). Iron(III) complexes with IS as ground state are rather rare although their existence is well documented.[2] The HS electronic configuration is adopted when relatively weak-field ligands are involved while the LS electronic ground state occurs when strong-field ligands are present. So, the majority of iron(III) compounds are HS or LS complexes.
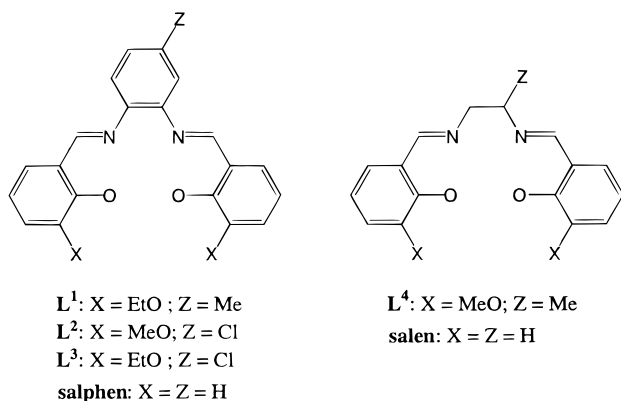
In addition, a relatively small number of six-coordinate iron(III) compounds can exhibit both the HS and LS configurations. A thermal LS ↔ HS spin transition occurs for these so-called spin-crossover compounds. The phenomenon is observed both in solution as well as in solid state. In the first case the

process is essentially molecular, owing to the isolation of molecules. In the solid state, the situation in general is quite different and involves cooperative character for the phenomenon. Cooperativity stems from the coupling between the intraionic electron-transfer $e_g \leftrightarrow t_{2g}$, the changing in the metal−ligand bond distance and the crystal lattice vibrations.[3]

(1) (a) Departamento de Química Inorgánica, Universidad de La Laguna. (b) Departamento de Física Fundamental y Experimental, Universidad de La Laguna. (c) Universidad de Santiago. (d) Universitat de Barcelona. (e) Universitat de València.

(2) (a) Martin, R. L.; White, A. H. *Inorg. Chem.* **1967,** *6,* 712. (b) Hoskins, B. F.; White, A. H. *J. Chem. Soc. A* **1970,** 1668. (c) Kostka, K. L.; Fox, B. G.; Hendrich, M. P.; Collins, T. J.; Richard, C. E. F.; Wright, L. J.; Munck, E. *J. Am. Chem. Soc.* **1993,** *115,* 6746. (d) Koch, S.; Holm, R. H.; Frankel, R. B. *J. Am. Chem. Soc.* **1975,** *97,* 6714. (e) Dolphin, D. H.; Sams, J. R.; Tsin, T. B. *Inorg. Chem.* **1977,** *16,* 711. (f) Summerville, D. A.; Cohen, I. A.; Hatano, K.; Scheidt, W. R. *Inorg. Chem.* **1978,** *17,* 2906. (g) Mansuy, D.; Morgenstern−Baradau, I.; Lange, M.; Gans, P. *Inorg. Chem.* **1982,** *21,* 1427. (h) Fritzgerald, J. P.; Haggerty, B. S.; Rheingold, A. L.; May, L.; Brewer, G. A. *Inorg. Chem* **1992,** *31,* 2006. (i) Kennedy, B. J.; Murray, K. S.; Zwack, P. R.; Homborg, H.; Kalz, W. *Inorg. Chem.* **1986,** *25,* 2539.

(3) (a) Cambi, L.; Szego, L. *Dtsch. Chem. Ges.* **1931,** *64,* 2591. (b) Cambi, L.; Cagnasso, A.; Atti, A. *Accad. Naz. Lincei, Cl. Sci. Fis. Mat Natl. Rend.* **1931,** 13, 809. (c) Gütlich, P. *Struct. Bonding (Berlin)* **1981,** 44, 83. (d) Gütlich, P.; Hauser, A.; Spiering, H. *Angew. Chem., Int. Ed. Engl.,* **1994,** 33, 2024. (e) König, E. *Struct. Bonding (Berlin)* **1991,** *76,* 51. (f) König, E. *Prog. Inorg. Chem.* **1987,** *35,* 527.

Chart 1

L^1: X = EtO ; Z = Me
L^2: X = MeO; Z = Cl
L^3: X = EtO ; Z = Cl
salphen: X = Z = H

L^4: X = MeO; Z = Me
salen: X = Z = H

The synthesis and characterization of six-coordinated iron(III) complexes with porphyrinate and Shiff base (SB) ligands have played a relevant role in the coordination chemistry of iron. The understanding of the factors which control the spin state in iron(III) has been a common objective. That is particularly important for iron(III)−porphyrinate complexes due to their biological relevance. The modelization of the prosthetic group of hemoproteins which display thermal spin equilibria is of current interest in understanding precisely how the protein structure tunes the electronic state of its prosthetic group and hence shifts the HS ↔ LS equilibrium.[4] In a similar fashion, concerning the iron(III)−SB coordination chemistry much emphasis has been focused on how chemical, structural, and bonding effects within the molecular species as well as intermolecular solid-state effects influence the crossover phenomenon. In this regard, six-coordinated iron(III) SB complexes are known to display a great variety of magnetic behaviors: minor variations in the components of the complexes (counterion, SB ligand substituents, structural features of the axial ligand, solvent molecules, and intermolecular effects in solid state) can lead either to HS, LS, or spin-crossover behavior.[5]

The present work reports on the synthesis, structural and magnetic characterization of new examples of iron(III)−SB complexes of general formula [Fe(L)(HIm)$_2$]Y (Chart 1). The reaction of Fe(L^1)Cl·H$_2$O (L^1 = N,N′-3,4-toluenebis(3-ethoxy-salicylideneimine), Fe(L^2)Cl·H$_2$O (L^2 = N,N′-4-chloro-o-phenylenebis(3-methoxysalicylideneimine), Fe(L^3)Cl·H$_2$O (L^3 = N,N′-4-chloro-o-phenylenebis(3-ethoxysalicylideneimine) and Fe(L^4)Cl·H$_2$O (L^4 = N,N′-1,2-propylenebis(3-methoxysalicylideneimine) with imidazole (HIm) in methanol led to the

hexacoordinated homo-bis-adducts of the iron(III)−SB system [Fe(L^1)(HIm)$_2$]Y (Y = ClO$_4^-$ (**1a**), PF$_6^-$ (**1b**) and BPh$_4^-$ (**1c**)), [Fe(L^2)(HIm)$_2$](ClO$_4$) (**2a**), [Fe(L^2)(HIm)$_2$](ClO$_4$)·H$_2$O (**2b**), [NaFe(L^2)(HIm)$_2$(ClO$_4$)$_2$] (**2c**), [Fe(L^3)(HIm)$_2$](ClO$_4$) (**3**), [Fe(L^4)-(HIm)$_2$](ClO$_4$) (**4a**), [Fe(L^4)(HIm)$_2$](BPh$_4$)·H$_2$O (**4b**) with the imidazole ligands occupying axial positions. The magnetic properties reveal that **1a**−**c**, **2a**, **3**, and **4b** are HS while **2c** is LS. Compounds **4a** and **2b**, display spin-crossover behavior. The crystal structures of **1a**, **2c**, and **4a** are also reported.

Experimental Section

Materials. All chemicals were reagent grade quality purchased from commercial sources and used as received. The Schiff base ligands L were prepared in a similar way to the literature method.[6] The starting complexes Fe(L)Cl·H$_2$O were prepared according to the method of Gerloch et al.[7] and recrystallized from acetone. The C, H, and N analyses were carried out on a Carlo Erba 1106 automatic analyzer.

Preparation of the Complexes. The syntheses of compounds **1a**−**c**, **2a**−**c**, **3** and **4a,b** were carried out in a similar fashion. A methanolic solution (25 mL) containing Fe(L)Cl·H$_2$O (0.168 mmol) and imidazole (2.98 mmol) was refluxed for 10 min and then filtered off while hot into a freshly prepared methanol solution (10 mL) of sodium perchlorate, hexafluorophosphate, or tetraphenylborate (1 mmol). The mixture was left to stand overnight. A black microcrystalline solid was collected, washed with small amounts of ice-cold methanol, and dried in air. Single crystals of **1a** and **4a** were grown from the reaction mixture.

A brown-red precipitate appeared when the refluxed mixture was added to the perchlorate solution in the particular case of **2**. It was separated by filtration. Two compounds crystallized from the resulting solution. In a first step a microcrystalline solid (**2b**) was formed. In a well-separated second step, prismatic black crystals of **2c** were formed after partial evaporation of the solution. The exposure of **2b** either under vacuum (ca. 10 mbars) at room temperature or heating at T > 345 K yielded the dehydrated compound **2a**. Thermal analysis revealed 2.5% loss of weight, which corresponds to one mole of water per molecular unit.

The chemical analysis data for **1**−**4** agree very well with the theoretical values. The data are available in the Supporting Information (Table S1).

Physical Measurements. Magnetic Susceptibility Measurements. The variable-temperature magnetic susceptibility measurements were carried out on polycrystalline samples over the temperature range 4.2−300 K with a fully automatized AZTEC DSM8 pendulum-type susceptometer equipped with a TBT continuous-flow cryostat and a Brüker BE15 electromagnet, operating at 1.8 T. The apparatus was calibrated with mercury tetrakis(thiocyanato)cobaltate(II). Experimental susceptibilities were corrected for diamagnetism of the constituent atoms by the use of Pascal's constants.

Structure Determinations. Data collections were carried out at 293 K on an Enraf-Nonius CAD4 four-circle diffractometer with graphite-monochromated Mo Kα radiation (λ = 0.710 69 Å), using the ω/2θ scan technique. Unit cell parameters were determined in each case from automatic centring of 25 reflections in the range 12 < θ < 21° for **1a** and **2c** (6.4 < θ < 12° for **4a**) and refined by least-squares method. Details concerning crystal data, data collection characteristics, and structure refinement are summarized in Table 1. Positional parameters for selected atoms are contained in Tables S3, S7 and S12 for **1a**, **2c**, and **4a**, respectively. Additional information on crystal data and experimental conditions are deposited as Supporting Information.

Totals of 6345, 4064, and 6853 reflections were measured in the range 2 < θ < 30°, 1.8 < θ < 27.5°, and 3 < θ < 29° for **1a**, **2c**, and **4a**, respectively; 5182, 4064, and 2887 of them were assumed as observed applying the conditions I > 2.5σ(I) (**1a**), I > 2σ(I) (**2c**), and I > 3σ(I) (**4a**). Three reference reflections were measured every 2 h

(4) (a) Geiger, D. K.; Lee, Y. J.; Scheidt, R. *J. Am. Chem. Soc.* **1984**, *106*, 9. (b) Scheidt, R.; Geiger, D. K.; Hayes, R. G.; Lang, G. *J. Am. Chem. Soc.* **1983**, *105*, 2625.
(5) (a) Federer, W. D.; Hendrickson, D. N. *Inorg. Chem.* **1984**, *23*, 3861. (b) Federer, W. D.; Hendrickson, D. N. *Inorg. Chem.* **1984**, *23*, 3870. (c) Timken, M. D.; Strouse, C. E.; Soltis, S. M.; Daveiro, S. R.; Hendrickson, D. N.; Abdel-Mawgoud, A. M.; Wilson, S. A. *J. Am. Chem. Soc.* **1986**, *108*, 395. (d) Timken, M. D.; Abdel-Mawgoud, A. M.; Hendrickson, D. N. *Inorg. Chem.* **1986**, *25*, 160. (e) Maeda, Y.; Oshio, H.; Takashima, Y. *Chem. Lett* **1982**, 943. (f) Oshio, H.; Maeda, Y.; Takashima, Y. *Inorg. Chem.* **1983**, *22*, 2684. (g) Matsumoto, N.; Ohta, S.; Yoshimura, C.; Ohyoshi, A.; Kohata, K.; Okawa, H.; Maeda, Y. *J. Chem. Soc., Dalton Trans.* **1985**, 2575. (h) Haddad, M. S.; Linch, M. W.; Federer, W. D.; Hendrickson, D. N. *Inorg. Chem.* **1981**, *20*, 123. (i) Haddad, M. S.; Federer, W. D.; Linch, M. W.; Hendrickson, D. N. *Inorg. Chem.* **1981**, *20*, 131. (j) Kennedy, B. J.; McGrath, A. C.; Murray, K. S.; Skelton, B. W.; White, A. H. *Inorg. Chem.* **1987**, *26*, 483. (k) Nishida, Y.; Kino, K.; Kida, S. *J. Chem. Soc., Dalton Trans.* **1987**, 1157. (l) Conti, A. J.; Chadha, R. K.; Sena, K. M.; Rheingold, A. L.; Hendrickson, D. N. *Inorg. Chem.* **1993**, *32*, 2670. (m) Conti, A. J.; Kaji, K.; Nagano, Y.; Sena, K. M.; Yumoto, Y.; Chadha, R. K.; Rheingold, A. L.; Sorai, M.; Hendrickson, D. N. *Inorg. Chem.* **1993**, *32*, 2681.

(6) Mederos, A.; Manrique, F. G.; Medina, A., *An. Quim.* **1980**, *76B*, 33.
(7) Gerloch M.; Lewis, J.; Mabbs F. E.; Richards A. *J. Chem. Soc. A* **1968**, 112.

Table 1. Crystallographic Data for Compounds **1a**, **2c**, and **4a**

	1a	**2c**	**4a**
empirical formula	$C_{31}H_{34}N_6O_8ClFe$	$C_{28}H_{24}N_6O_{12}Cl_3NaFe$	$C_{25}H_{28}N_6O_8ClFe$
a, Å	10.609(3)	14.969(6)	12.402(2)
b, Å	10.762(3)	17.324(6)	14.354(2)
c, Å	15.043(3)	13.050(10)	15.773(2)
α, deg	105.13(2)	90	90
β, deg	90.67(2)	100.85(6)	90
γ, deg	102.09(2)	90	90
V, Å^3	1617.2(8)	3324(3)	2808(1)
Z	2	4	4
fw	709.94	821.72	631.83
space group	$P1$	$C2/c$	$P2_12_12_1$
temp, K	293	293	293
ρ_{calc}, g cm^3	1.458	1.642	1.495
μ, cm^{-1}	7.20	7.80	6.91
final R indices [$I > 2\sigma(I)$]	0.0636, 0.1369	0.0556, 0.1294	0.1025, 0.2529
R indices (all data)	0.1752, 0.2234	0.1545, 0.2192	0.2788, 0.3633

^{a} $R = \sum||F_o| - |F_c||/\sum|F_o|$; $R_w = [\sum w(|F_o| - |F_c|)^2/\sum w|F_o|^2]^{1/2}$.

as orientation and intensity control, significant intensity decay was not observed. Lorentz and polarization corrections were made for **1a**, **2c**, and **4a**. Absorption correction was made for **4a**. The structures were solved using the SHELXS-86[8] computer program and refined by full-matrix least-squares method with the SHELX76, SHELXL93, and SDP computer program.[9] Calculations of geometrical parameters were made with PARST,[10] and molecular graphics were made with ORTEPII.[11]

The perchlorate and the chloride atoms appear to be disordered, for **2c**. So, the occupancy parameters of their atoms were calculated. All non-hydrogen atoms were computed and refined with an overall isotropic temperature factor using a riding model. Final refinement converged to $R = 0.064$ (**1a**) and 0.056 (**2c**) for all observed reflections. The number of refined parameters was 179 (**1a**) and 274 (**2c**).

The perchlorate geometry is not clearly resolved for **4a**. The best configuration, around the Cl position, gives statistical disorder with three O positions fully occupied and two others with partial occupancy. The bond lengths remain coherent but angles are not significant. The disorder seems to be of the dynamic type according to the elongated form of the thermal ellipsoids; the O(11) and O(12) oxygen atoms are refined with 0.70 and 0.30 occupancy factors, respectively. Fe and Cl atoms and the O and N atoms coordinated to the metal were refined with anisotropic displacement parameters. The remaining atoms were isotropically refined. Hydrogen atoms were calculated at idealized positions and introduced into the structure-factors calculations. Empirical absorption correction (minimum and maximum corrections being 0.97 and 1.01, respectively) and extinction correction (extinction coefficient 3.029×10^{-8}) were applied. Refinement converged at $R = 0.103$ with a final shift-to-error ratio of 0.001. The most intense peak in the final Fourier map had a height of 1.48 e Å^{-3}, and the minimum negative peak had a depth of -0.89 e Å^{-3}, both near the Fe atom. As a result of the weak diffracting power of the crystal, only a small fraction of reflections (about 25%) were observed, and thus no anisotropic thermal parameters were used for the majority of the atoms of the ligands. The poor quality of the crystal is largely responsible for the high value of the R factors. The structural disorder of the perchlorate anion, and the large thermal oscillations or positional disorder indicated by larger-than-normal mean-square displacement parameters of the many atoms also contribute to the relatively high R factors.

(8) Sheldrick, G. M., SHELXS86. *Acta Cryst*allogr. **1990**, *A46*, 467.
(9) (a) Sheldrick, G. M. *SHELX-76: A computer program for crystal structure determination*; University Cambridge: Cambridge, 1976. (b) Sheldrick, G. M. *SHELXL93: Program for the Refinement of Crystal Structures*; University of Göttingen: Germany, 1993. (c) *SDP/VAX*, V.2.2; Enraf-Nonius: College Station, TX, and Delft, The Netherlands, 1985.
(10) Nardelli M. PARST. *Comput. Chem.* **1983**, *7*, 95.
(11) Johnson, C. K. *ORTEPII*; Report ORNL-5138; Oak Ridge National Laboratory: Oak Ridge, TN, 1976.

Results and Discussion

X-ray Structures of 1a, 2c and 4a. Figures 1, 2, and 3 show the molecular structures of the complexes **1a**, **2c**, and **4a** along with the atomic numbering scheme used for all non-hydrogen atoms. Selected bond distances and angles are listed in Table 2. The lattices of **1a** and **4a** are made up of $[Fe(L^1)(HIm)_2]^+$ and $[Fe(L^4)(HIm)_2]^+$ cations, respectively, and uncoordinated perchlorate anions. The cationic complex is six-coordinate, the equatorial plane being occupied by the SB and the axial positions by the imidazole ligands. The iron(III) atom lies approximately within this plane defined by the four donor atoms of the SB, it is 0.005 Å out of this plane. The coordination environment of the metal ion atom is defined by a distorted octahedral geometry the angles N(1)−Fe−O(2), N(2)−Fe−O(1), N(3)−Fe−N(4) deviating markedly from the ideal value of 180° [166.9(1), 166.9(1), 173.2(1)° (**1a**) and 167.8(4), 166.8(4), 175.9(4)° (**4a**)]. In the case of **4a** the C(8) and C(9) atoms are −0.21 and 0.22 Å, respectively, out of the FeN_2C_2 least-squares plane which adopts a gauche conformation typical of the salen complexes.[5k,12,13] Compound **2c** is made up of neutral [Fe−Na] dinuclear entities. The iron atom is coordinated to the [N_2O_2] SB donor atoms set, which defines the equatorial plane, and to two imidazole ligands filling the axial positions as in **1a** and **4a**. The sodium atom is surrounded by six oxygen atoms belonging to two phenoxo bridging groups, two methoxy substituents and two perchlorate anions. The six oxygen atoms around the sodium atom define a very distorted octahedral geometry.

Previous studies on hexacoordinated iron(III) complexes with a N_4O_2 donor set have revealed that the bond distances and angles of the iron atom are sensitive to its spin state.[13−15] The HS-to-LS spin state change involves depopulation of the e_g orbitals, which have an antibonding character. This change is concomitant with the shortening of the iron-to-ligand bond distances. The largest variation is observed in the iron−nitrogen ones being significantly smaller in the LS form. However, the iron−oxygen bond length is almost constant irrespective of the spin state of the iron(III). This is consistent with the π-donor character of the phenoxo groups.[12]

(12) Maeda, Y.; Takashima, Y. Matsumoto, N.; Ohyoshi, A. *J. Chem. Soc., Dalton Trans.* **1986**, 1115.
(13) Kennedy, B. J.; McGrath, A. C.; Murray, K. S.; Snow, M. R. *Inorg. Chem*. **1985**, *24*, 1645.
(14) Kitaura, E.; Nishida, Y.; Okawa, H.; Kida, S. *J. Chem. Soc., Dalton Trans.* **1987**, 3055.
(15) Kennedy, B. J.; Fallon, G. D.; Gatehouse, B. M.; Murray, K. S. *Inorg. Chem.* **1984**, *23*, 580.
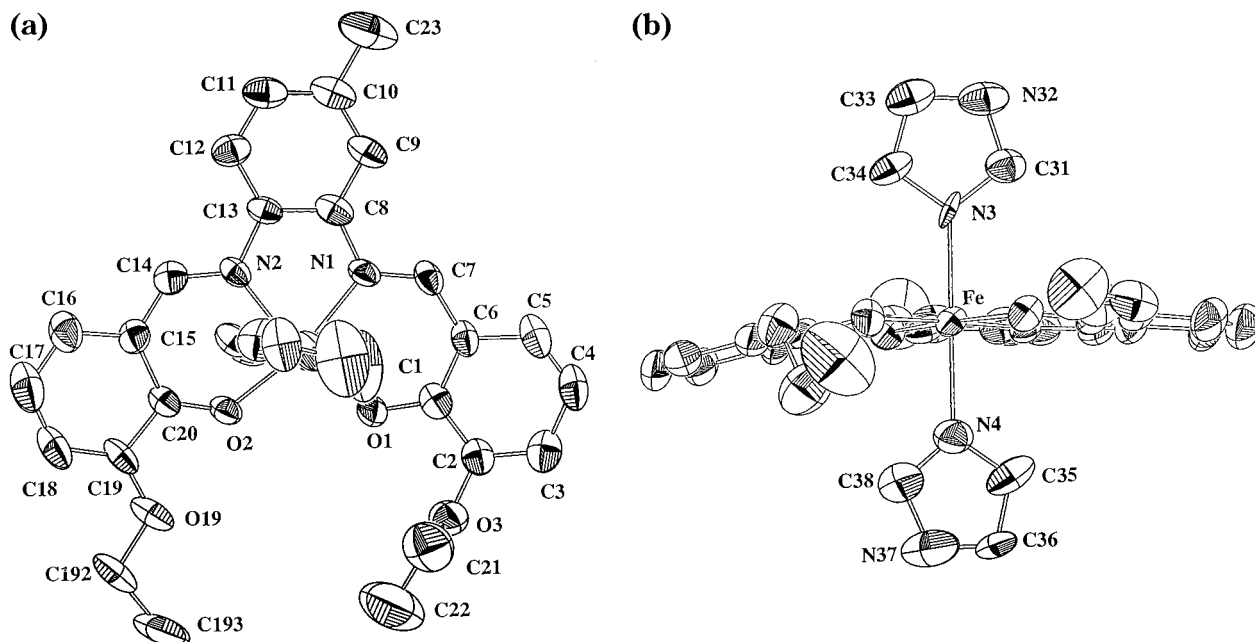
Figure 1. Top (a) and side (b) views of the molecular structure of **1a** (50% probability displacement ellipsoids).
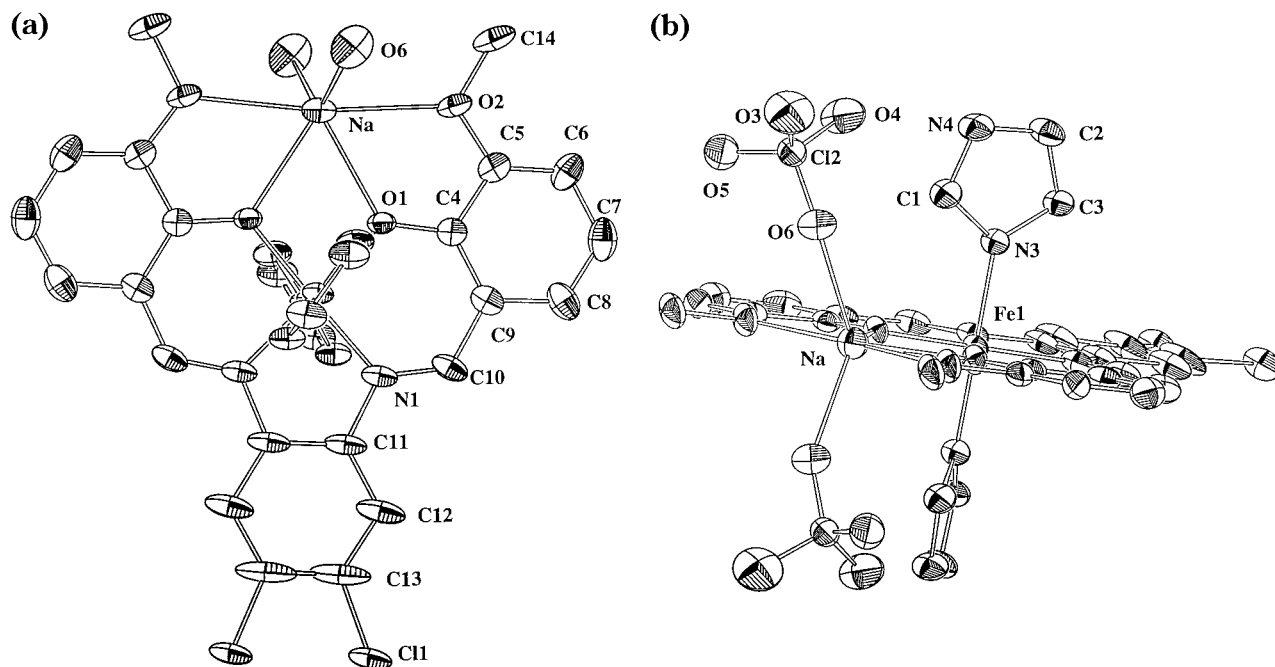

Figure 2. Top (a) and side (b) views of the molecular structure of **2c** (50% probability displacement ellipsoids).

Table 3 lists the average Fe−N(imine), Fe−N(imidazole), Fe−O, and Fe−N bond distances of **1a**, **2c**, and **4a** and the related complexes **i**−**vi** together with their spin state. The average Fe−N(HIm) distances are longer than the Fe−N(imine) distances [2.148 and 2.123 Å against 2.105 and 2.090 Å] for **1a** and **4a**, respectively. Both are consistent with the reported bond lengths for similar HS iron(III)−SB complexes. In contrast, the average iron−nitrogen distance for **2c** [Fe−N = 1.935 Å] is significantly shorter than that of **1a** and **4a** being close to those of iron(III) LS complexes. As stated above, the average Fe−O distance is insensitive to the spin state of the iron(III) being almost constant for both HS and LS complexes: 1.899, 1.874, and 1.919 Å for **1a**, **2c**, and **4a**, respectively.[5j,k] In light of these structural features, it can be concluded that complexes **1a** and **4a** are HS and that **2c** is LS at room

temperature. These results are consistent with the magnetic susceptibility measurements (vide infra).

The relative orientation of the imidazole rings is one of the parameters which determine the coordination core bond lengths. It controls the metal-to-imidazole π-back-bonding and consequently, the efficiency of the LS state stabilization. Efficient d_π−p_π overlap is achieved when the two planes defined by the imidazole rings are orthogonal and orientated along the two N−Fe−O diagonals of the equatorial coordination frame. In contrast, decoupling of the d_π−p_π overlap occurs when the imidazole rings bisect the angles defined by the two N−Fe−O diagonals. Hence the capacity to stabilize the LS state decreases. Concerning **2c**, the two imidazole ligands define a dihedral angle of 79° and their projections on the equatorial plane lie along the O−Fe−N diagonals. So, their relative orientations cor-
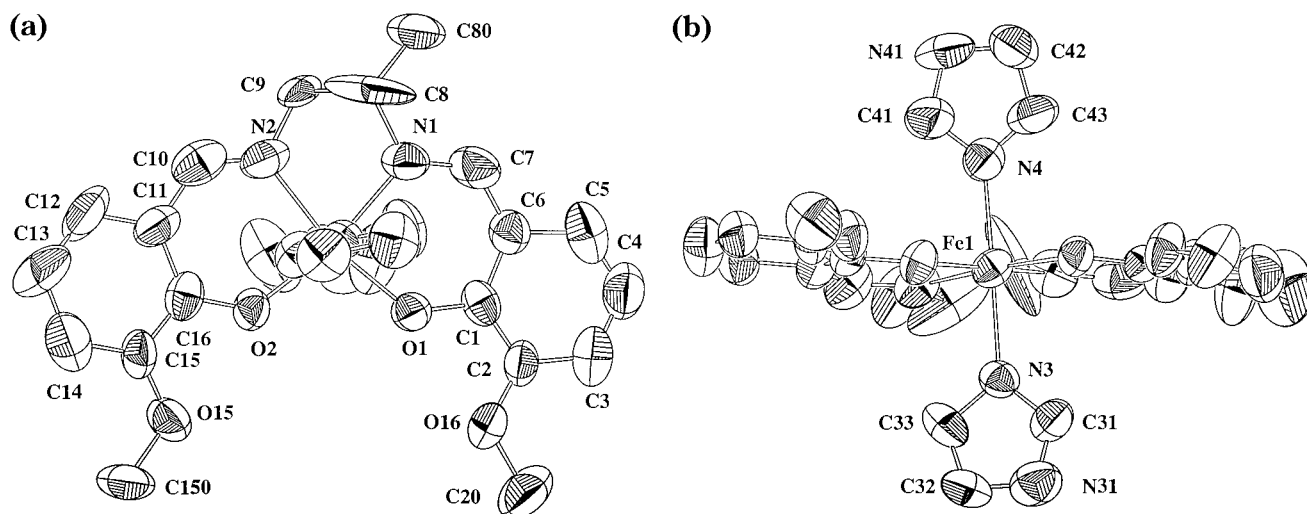
(a)

(b)

Figure 3. Top (a) and side (b) views of the molecular structure of **4a** (50% probability displacement ellipsoids).

Table 2. Selected Bond Distances (Å) and Angles (deg) for **1a**, **2c**, and **4a**

1a		2c		4a	
Fe−N(1)	2.098(3)	Fe−N(1)	1.896(2)	Fe−N(1)	2.102(10)
Fe−N(2)	2.112(3)	Fe−N(3)	1.975(2)	Fe−N(2)	2.079(11)
Fe−N(3)	2.127(2)	Fe−O(1)	1.874(2)	Fe−N(3)	2.109(10)
Fe−N(4)	2.169(3)	Na−O(1)	2.376(2)	Fe−N(4)	2.137(8)
Fe−O(1)	1.906(2)	Na−O(6)	2.404(2)	Fe−O(1)	1.919(7)
Fe−O(2)	1.893(3)	Na−O(2)	2.500(3)	Fe−O(2)	1.919(8)
		Fe−Na	3.451(2)		
N(3)−Fe-N(4)	173.2(1)	N(1)−Fe-O(1)	96.30(9)	N(3)−Fe-N(4)	175.9(4)
N(2)−Fe-O(1)	166.9(1)	N(1)−Fe−N(1)*	85.60(12)	N(2)−Fe-O(1)	166.8(4)
N(1)−Fe-O(2)	166.9(1)	O(1)*-Fe−O(1)	81.80(10)	N(1)−Fe-O(2)	167.8(4)
N(2)−Fe-N(1)	77.4(1)	N(3)−Fe-N(1)	90.94(8)	N(2)−Fe-N(1)	77.9(5)
N(1)−Fe-O(1)	89.6(1)	N(3)−Fe-O(1)	90.04(7)	N(1)−Fe-O(1)	89.1(4)
N(2)−Fe-O(2)	89.5(1)	O(1)*-Fe−N(1)	177.97(7)	N(2)−Fe-O(2)	90.1(4)
N(3)−Fe-O(2)	87.8(1)	N(3)−Fe-O(1)*	89.78(7)	N(3)−Fe-O(2)	90.2(3)
N(3)−Fe-N(1)	88.1(1)	N(3)−Fe-N(1)*	89.23(8)	N(3)−Fe-N(1)	87.9(4)
N(3)−Fe-O(1)	91.9(1)	N(3)−Fe-N(3)*	179.76(9)	N(3)−Fe-O(1)	91.6(3)
N(3)−Fe-O(2)	91.9(1)	O(1)−Na-O(1)*	62.18(9)	N(3)−Fe-O(2)	90.5(4)
N(4)−Fe-N(2)	87.2(1)	O(2)−Na-O(2)*	171.95(9)	N(4)−Fe-N(2)	86.9(5)
N(4)−Fe-N(1)	86.4(1)	O(6)−Na-O(6)*	126.16(12)	N(4)−Fe-N(1)	88.4(4)
N(4)−Fe-O(1)	92.0(1)	O(1)−Na-O(6)	107.06(8)	N(4)−Fe-O(1)	90.2(4)
N(4)−Fe-O(2)	92.6(1)	O(1)*-Na−O(6)	118.82(7)	N(4)−Fe-O(2)	93.0(4)
O(1)−Fe-O(2)	103.6(1)	O(1)−Na-O(2)*	125.08(7)	O(1)−Fe-O(2)	103.0(3)
		O(1)−Na-O(2)	62.97(6)		
		O(6)−Na-O(2)*	96.30(8)		
		O(6)−Na-O(2)	80.02(8)		

Table 3. Average Iron−Ligand Bond Distances (Å) for **1a**, **2c**, **4a**, and Some Related Compounds (**i**−**vi**).

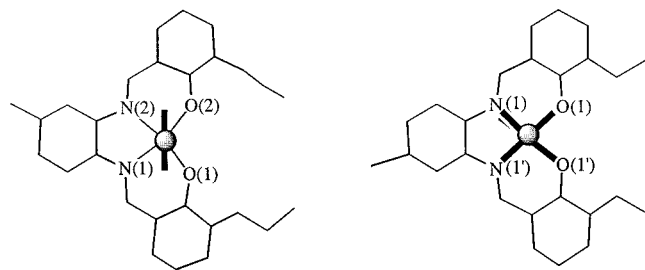| compound	Fe−N(SB)	Fe−O(SB)	Fe−N(Him)	Fe−N[a]	spin state	ref
1a	2.105	1.899	2.148	2.126	HS	this work
2c	1.896	1.874	1.975	1.935	LS	this work
4a	2.090	1.919	2.123	2.106	LS ↔ HS	this work
i [Fe(acen)(Him)$_2$](BPh$_4$)	1.899	1.920	1.990	1.944	LS	5k
ii [Fe(salen)(Him)$_2$](ClO$_4$)H$_2$O	2.108	1.917	2.143	2.125	HS	5k
iii [Fe(salphen)(Him)$_2$](BPh$_4$)	2.125	1.896	2.165	2.145	HS	5k
iv [Fe(salen)(Him)$_2$](ClO$_4$)	1.913 (LS)	1.903 (LS)	1.991 (LS)	1.952 (LS)	LS ↔ HS	5j
	2.067 (HS)	1.901 (HS)	2.146 (HS)	2.106 (HS)		
v [Fe(salen)(Him)$_2$](BF$_4$)	2.072	1.901	2.122	2.097	LS ↔ HS	5j
vi [Fe(salen)(Him)$_2$](PF$_6$)	2.135	1.903	2.153	2.144	HS	5j

[a] Fe−N represents the average iron−nitrogen [N(SB)−N(Him)] bond distances.

respond to that of the former situation (see Chart 2, right); interestingly **2c** is LS. The two imidazole ligands define dihedral angles of 10.5 and 21.4° for **1a** and **4a**, respectively. Their projections bisect the O(2)−Fe−N(2) and O(1)−Fe−N(1) equatorial angles and fit well with the latter situation (see Chart 2, left); **1a** and **4a** are HS at room temperature. Furthermore,

the dihedral angle between the imidazole ligands is significantly greater for **4a** than that for **1a**. Interestingly, **4a** undergoes HS ↔ LS spin transition at low temperatures, being almost LS at 40 K.

So, the spin state of **1a**, **2c**, and **4a** (at room temperature) and the relative orientation of the imidazole rings agree with

Chart 2

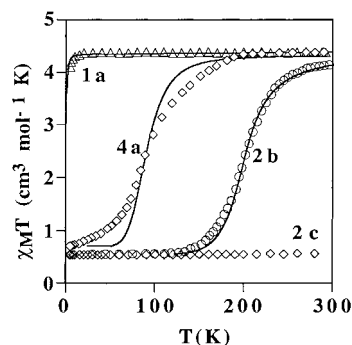**Figure 4.** $\chi_M T$ product versus T plot for **1a**, **2b**, **2c**, and **4a**. The solid lines correspond to the calculated data (see text).
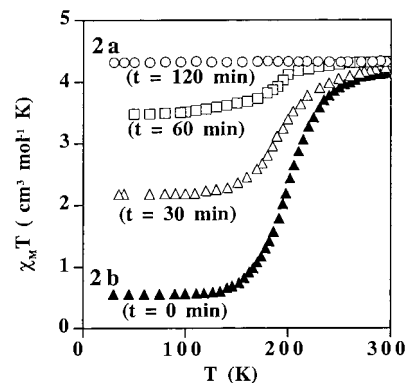

Figure 5. Dependence of the $\chi_M T$ product versus T on the degree of dehydratation for **2b**. The duration of vacuum pumping is indicated in parentheses.

that stated above. However, it should be noted that small structural changes other than the relative orientation of the imidazole groups can provoke also drastic changes on the spin state of the complex.

Finally, it should be noted that the predisposition of compounds in Table 3 to undergo spin conversion seems to be reflected on the Fe−N bond distances. In fact, the **4a**, **iv**, and **v** spin-crossover compounds display shorter average Fe−N bond distances than the **1a**, **ii**, **iii**, and **vi** HS compounds.

Magnetic Properties. Figure 4 shows the thermal variation of the $\chi_M T$ product (χ_M being the molar magnetic susceptibility and T the temperature) for **1a**, **2c**, **2b**, and **4a**. The $\chi_M T$ value for **1a** at room temperature is 4.33 cm³ mol⁻¹ K and it remains constant up to 20 K. Then, it decreases smoothly, most likely due to a small zero-field splitting (zfs) and/or intermolecular interactions. This magnetic behavior is satisfactorily matched through the axial $S = {}^5/_2$ zfs Hamiltonian, $\mathbf{H} = D[\mathbf{S}_z^2 - (1/3)S(S+1)] + g\beta\mathbf{HS}]$, with $g = 1.99$ and $D = |0.8 \text{ cm}^{-1}|$. Similar behavior was observed for compounds **1b**, **1c**, **3**, and **4b**, revealing that they are HS. In contrast, **2c** is LS: the $\chi_M T$ product equal to 0.55 cm³ mol⁻¹ K remains constant following a Curie law for an $S = {}^1/_2$ ground state with $g = 2.4$ in the temperature range investigated.

The $\chi_M T$ product for **2b** and **4a** is equal to 4.14 and 4.33 cm³ mol⁻¹ K, respectively, being close to what is expected for a HS iron(III) complex. They slowly decrease upon cooling to $\chi_M T = 0.55$ cm³ mol⁻¹ K which corresponds to the LS ground state. This behavior is characteristic of a continuous $S = {}^1/_2 \leftrightarrow S = {}^5/_2$ spin-crossover phenomenon. The warming mode shows no detectable thermal hysteresis. The temperature, $T_{1/2}$, at which 50% of molecules are in the LS state is 202 and 91 K for **2b** and **4a**, respectively.

Thermodynamical parameters associated with the spin crossover process can be estimated applying the model of Slichter and Drickamer.[17] This model is based on the assumption that high-spin and low-spin molecules are statistically distributed and form regular solutions. At equilibrium, this model leads to the implicit equation

$$\text{Ln}\left(\frac{1 - C_{HS}}{C_{HS}}\right) = \frac{\Delta H + \Gamma(1 - 2C_{HS})}{RT} - \frac{\Delta S}{R} \quad (1)$$

Here, Γ is a term that reflects the strength of the cooperative intermolecular interactions. The high-spin molar fraction, C_{HS}, is calculated at each temperature from the magnetic measurements using

$$C_{HS} = [\chi_M T - (\chi_M T)_{LS}]/[(\chi_M T)_{HS} - (\chi_M T)_{LS}] \quad (2)$$

The values for pure HS and LS forms, $(\chi_M T)_{HS}$ and $(\chi_M T)_{LS}$,

are taken from the experimental magnetic data. There is a good agreement between the experimental and calculated data for **2b** (see Figure 4). The parameters obtained from simulation are $\Delta H = 12$ kJ mol⁻¹, $\Gamma = 1.6$ kJ mol⁻¹ and $\Delta S = 60$ J mol⁻¹ K⁻¹.

Concerning **4a**, the experimental $\chi_M T$ data suggest that LS ↔ HS conversion kinetics strongly depends on C_{HS}. These values are significantly smaller than the calculated at temperatures greater than $T_{1/2} = 91$ K for the reasonable set of parameters $\Delta H = 5.46$ kJ mol⁻¹, $\Gamma = 0$, and $\Delta S = 60$ J mol⁻¹ K⁻¹ (see solid line **4a** in Figure 4). The reverse is observed for temperatures smaller than $T_{1/2} = 91$ K. This fact might indicate that the HS-to-LS process experiences acceleration or retardation depending on which the nature of the dominant phase is HS or LS, respectively. The ΔH and ΔS values estimated for **2b** and **4a** are close to those found for other iron(III) spin-crossover complexes.[5f,5j,5m,18]
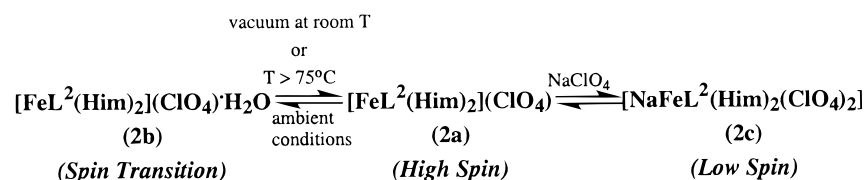
Interestingly, **2b** easily loses the crystallization water molecule to yield the anhydrous species **2a**. Water loss occurs either at $T > 345$ K or in vacuo at room temperature. Figure 5 displays the influence of the dehydratation degree of **2b** on its magnetic behavior. The spin conversion is gradually more incomplete and vanishes as the water loss process is completed. This happens when **2b** stands in vacuo more than 2 h at room temperature. It is clear from these results that the loss of the lattice water molecule induces the disappearance of the spin crossover phenomenon. The hydratation−dehydratation process is fully reversible. So, exposure of **2a** to ambient atmosphere for a few hours yields **2b**. This process can be repeated as many times as required without any detectable variation in their magnetic properties.

(16) Fukuya, M.; Ohba, M.; Motoda, K.; Matsumoto, N.; Okawa, H.; Maeda, Y. *J. Chem. Soc., Dalton Trans.* **1993**, 3277.
(17) Slichter, C. P.; Drickamer, H. G. *J. Chem. Phys* **1972**, *56*, 2142.

(18) Sorai, M.; Nagano, Y.; Conti, A. J.; Hendrickson, D. N. *J. Phys. Chem. Solids* **1994**, *55*, 317.

Scheme 1

$$[FeL^2(Him)_2](ClO_4)\cdot H_2O \underset{\substack{\text{ambient} \\ \text{conditions}}}{\overset{\substack{\text{vacuum at room T} \\ \text{or} \\ T > 75^oC}}{\rightleftarrows}} [FeL^2(Him)_2](ClO_4) \underset{}{\overset{NaClO_4}{\rightleftarrows}} [NaFeL^2(Him)_2(ClO_4)_2]$$

$$\textbf{(2b)} \qquad\qquad\qquad\qquad \textbf{(2a)} \qquad\qquad\qquad\qquad \textbf{(2c)}$$

$$\textit{(Spin Transition)} \qquad\qquad \textit{(High Spin)} \qquad\qquad \textit{(Low Spin)}$$

It is well-known that uncoordinated solvent molecules can influence the spin crossover behavior.[3c,d] The spin conversion is an intraionic $e_g \leftrightarrow t_{2g}$ electron tranfer process coupled with changes in shape and size of the complex. The spin crossover phenomenon strongly depends on the efficacity of transmitting these changes in the whole crystal. Water molecules can participate to intermolecular hydrogen bonds enhancing the cooperative nature of the spin conversion and/or modulating the ligand field strength which controls the spin state of the metal ion.[19] In the present case, hydrogen bonding might involve the water molecule, the noncoordinated NH group of the imidazole ligand and/or the SB chlorine substituent.

Another interesting chemical aspect of **2a** is that this compound is able to act as ligand toward the sodium cation to transform into **2c** and curiously, **2c** is a low-spin iron(III)

species. The spin state of complex **2a**, as well as that of its adducts (**2b** and **2c**) are summarized in Scheme 1.

Supporting Information Available: Tables S1−S15, giving complete list of chemical analysis (calculated and experimental data for compounds **1a**−**c**, **2a**−**c**, **3**, and **4a,b**), additional crystallographic data, atomic coordinates and equivalent isotropic displacement parameters, bond lengths and angles, anisotropic thermal parameters, and hydrogen atom locations (23 pages). Ordering information is given on any current masthead page.

IC980297Q

(19) Claude, R.; Zarembowitch, J.; Philoche-Levisalles, M.; D'Yvoise, F. *New. J. Chem.* **1991**, *15*, 635.